Cell Reports
Resource

Characterization and Analysis of the Composition and Dynamics of the Mammalian Riboproteome

Markus Reschke,[1,5] John G. Clohessy,[1,5] Nina Seitzer,[1] Daniel P. Goldstein,[1] Susanne B. Breitkopf,[2] Daniel B. Schmolze,[3] Ugo Ala,[1,4] John M. Asara,[2] Andrew H. Beck,[3] and Pier Paolo Pandolfi[1,*]
[1]Cancer Genetics Program, Department of Medicine and Pathology, Beth Israel Deaconess Medical Center, Harvard Medical School, Boston, MA 02215, USA
[2]Division of Signal Transduction, Beth Israel Deaconess Medical Center, Department of Medicine, Harvard Medical School, Boston, MA 02215, USA
[3]Department of Pathology, Beth Israel Deaconess Medical Center and Harvard Medical School, Boston, MA 02215, USA
[4]Molecular Biotechnology Center and Department of Genetics, Biology, and Biochemistry, University of Turin, 10124 Turin, Italy
[5]These authors contributed equally to this work
*Correspondence: ppandolf@bidmc.harvard.edu
http://dx.doi.org/10.1016/j.celrep.2013.08.014

SUMMARY

Increasing evidence points to an important role for the ribosome in the regulation of biological processes and as a target for deregulation in disease. Here, we describe a SILAC (stable isotope labeling by amino acids in cell culture)-based mass spectrometry approach to probing mammalian riboproteomes. Using a panel of cell lines, as well as genetic and pharmacological perturbations, we obtained a comparative characterization of the cellular riboproteome. This analysis identified a set of riboproteome components, consisting of a diverse array of proteins with a strong enrichment for RNA-binding proteins. Importantly, this global analysis uncovers a high incidence of genetic alterations to riboproteome components in cancer, with a distinct bias toward genetic amplification. We further validated association with polyribosomes for several riboproteome components and demonstrate that enrichment at the riboproteome can depend on cell type, genetics, or cellular stimulus. Our results have important implications for the understanding of how ribosomes function and provide a platform for uncovering regulators of translation.

INTRODUCTION

For many years now, gene expression has been measured as a reflection of transcriptional activation, and the assumption has been made that the absolute level of mRNA for a given gene within the cell directly correlates with protein level for that gene. Although mRNA level strongly correlates with protein expression, more recent evidence highlights the very important role that posttranscriptional events, including translation and microRNA (miRNA) regulation of mRNA, play in regulating gene expression (Xue and Barna, 2012; Fabian and Sonenberg, 2012). Similar to key regulators of gene transcription (e.g., p53 or c-Myc), key regulators of translation are specifically targeted in human diseases, including cancer. Indeed, recent data suggest that RNA binding proteins (RBPs) are frequently associated with disease. For example, Fragile-X mental retardation protein is involved in Fragile-X syndrome and autism (Darnell et al., 2011), proteins such as musashi-1 and -2 are involved in stem cell biology and leukemia (Kharas et al., 2010), and the *NPM1* gene is frequently translocated and mutated in a variety of hematological malignancies (Grisendi et al., 2006). Additionally, deficiency and mutation of ribosome and ribosome biogenesis proteins themselves are associated with disease and developmental abnormalities, including Diamond-Blackfan anemia, Shwachman-Diamond syndrome, and X-linked dyskeratosis congenita (Narla and Ebert, 2010). However, a more global approach to systematically determine in greater detail the players that coordinate translation is currently lacking. Such an approach will, in turn, enable the identification of key regulators of translation in specific conditions and help better elucidate the role that these proteins play in disease pathology.

The majority of actively translating ribosomes exist in the cell as polysomes, multiple ribosomes loaded on mRNAs to direct translation. However, the process of priming RNA for translation, subsequent loading of ribosomes, and efficient translation require a significant number of extraribosomal factors including initiation/elongation factors and RNA helices that are critical to efficient translation (Jackson et al., 2010). Thus, it is likely that many players required for correct translation remain to be uncovered, and this represents a major bottleneck to understanding, in depth, exactly how translation is coordinated.

Here, we applied a SILAC (stable isotope labeling by amino acids in cell culture)-based mass spectrometry approach to comprehensively characterize the proteins that constitute the actively translating ribosome, i.e., the riboproteome, as defined (1) by the proteins associated with the ribosome itself, and which may be required for either directing translation or quality control

of nascent proteins, and (2) by the proteins associated with mRNAs undergoing active translation.

By employing this high-throughput approach to the analysis of proteins associated with actively translating polysomes in various cellular populations and under varying conditions, we were able to obtain a comprehensive overview of the riboproteome. We demonstrate the power of this approach to identify differential riboproteome components among cancer cell lines and in the analysis of genetic and pharmacological perturbations to the riboproteome. This has allowed us to present a detailed characterization of the prostate riboproteome and to highlight the diversity of proteins that are associated with actively translating polysomes. Our data identify a number of components of the riboproteome and demonstrate the ability of this approach to address the dynamic nature of the riboproteome upon specific perturbations. Furthermore, this platform will enable us to gain important insights to the makeup of the riboproteome and will help identify important factors associated with translational regulation.

RESULTS

High-Throughput Analysis of the Riboproteome Using a SILAC-Based Approach

We hypothesize that the process of active translation within the cell is regulated by a multitude of proteins that can interact with either the ribosome itself, the mRNAs that are being actively translated, or proteins that may have the capacity to interact with both the ribosome and mRNA.

In order to characterize the components that constitute the actively translating ribosome (i.e., the riboproteome), we applied a mass spectrometry approach to quantitatively evaluate the protein components that are differentially associated with translation in different cellular contexts, while also allowing for a comprehensive overview of the proteins that make up the riboproteome.

To this end, we cultured relevant cell lines of both mouse (e.g., mouse embryonic fibroblasts [MEFs]) and human origin (e.g., prostate cancer cell lines) with SILAC media to incorporate amino acids for light (Lys_0^{C13}; Arg_0^{N14}) or heavy (Lys_6^{C13}; Arg_{10}^{N15}) labeling of proteins, achieving a labeling efficiency of greater than 95% (Table S1), and proceeded to isolate riboproteome components as outlined in Figure 1A. Labeled cells were seeded to ensure subconfluency at harvesting and were treated with 100 μg/ml cycloheximide prior to harvesting (see Experimental Procedures). Cells were collected in PBS containing cycloheximide, and equal amounts of cell lysates were loaded on 15%–50% sucrose gradients. Polysomes were separated by density gradient centrifugation and collected by fractionation (Figure S1A). Protein from individual polysome fractions was precipitated by deoxycholate-TCA precipitation and resuspended in buffer (0.1 M Tris [pH 8.8]; 1% SDS). Precipitated protein from fractions containing polysomes for heavy and light-labeled cells were combined in a ratio of 1:1 (v/v) and run on an SDS-PAGE gel, which was subsequently stained using Coomassie brilliant blue. The gel lane was cut into eight separate pieces and submitted to the BIDMC Mass Spectrometry Core for analysis by microcapillary liquid chromatography-tandem mass spectrometry (LC-MS/MS) analysis on a hybrid linear ion trap-orbitrap mass spectrometer. All resulting MS data were further processed with Mascot or Andromeda and the MaxQuant software suite as previously described (Cox and Mann, 2008; Cox et al., 2011).

This whole procedure required considerable optimization, as preliminary experiments identified extensive protease activity in polysomal fractions, resulting in degradation to ribosomal components and affecting quality of mass spectrometry results (Figure S1B). In order to resolve these issues, we employed a comprehensive array of protease inhibitors (as detailed in Experimental Procedures), which completely eliminated such protease activity and degradation artifacts.

To uncover the riboproteomic diversity within cellular populations, we applied this approach to a number of cell systems that included both relevant human prostate cell lines (Du145, PC3, PPC1 prostate cancer cell lines, and the immortalized prostatic epithelial cell lines PWR1E and RWPE1) and MEFs (immortalized *Npm1* wild-type and null) as outlined in Figures 1A and S1C.

Initially, we compared actively translating polysomes from the normal prostatic epithelial cell lines PWR1E and RWPE1 (two immortalized cell lines routinely used as normal controls for prostate cancer studies) with the metastatic prostate cancer cell line Du145 (Figure S1C). Second, we compared the riboproteomes of the prostate cancer cell lines Du145 and PC3. The use of these four cell lines allowed us to evaluate how the riboproteome changes from a relatively normal situation (PWRE1, RWPE1) to a cancerous state (Du145) and between two different cancer cell lines that harbor distinct genetic alterations (Du145 $PTEN^{wt};TP53^{mut}$ and PC3 $PTEN^{null};TP53^{null}$) (Figure S1C). Third, we compared the riboproteomes of PPC1 prostate cancer cells ($PTEN^{null};TP53^{null}$) treated with the mTOR inhibitors rapamycin and PP242 (Figure S1C). Finally, we compared MEFs harboring wild-type or null alleles for the ribosome biogenesis gene *Npm1* (Figure S1C).

These data allowed us to determine the overall composition of the ribosome and its associated proteins and evaluate quantitative differences in components of the mammalian riboproteome. Importantly, an initial comparison between polysomes derived from Du145 heavy- and light-labeled cells revealed that all quantified proteins showed an average Log_2 (H/L) ratio of around 0 (226 quantified proteins; mean 0.0029, SD ±0.1866) (Figure 1B; Table S2), demonstrating that differences observed between cell lines do not arise from variations in sample preparation and confirming both reliability as well as reproducibility of the technique.

In further support of this approach as a method to study composition and quantitative differences among riboproteomes, a comparison of the two normal and cancer cell line (hereafter referred to as N/C) data sets revealed a substantial overlap in identified proteins from immortalized normal epithelial cell lines, with a significant positive correlation ($R^2 = 0.4662$, $p = < 0.0001$). This demonstrates that these normal cell lines share significant similarity, which, in turn, gives greater significance to differences that exist between normal and cancer riboproteomes (Figure 1C).

Importantly, we detected several differences between the riboproteomes of N/C data sets as well as between cancer cell types (hereafter referred to as C/C) using indicated cutoff values

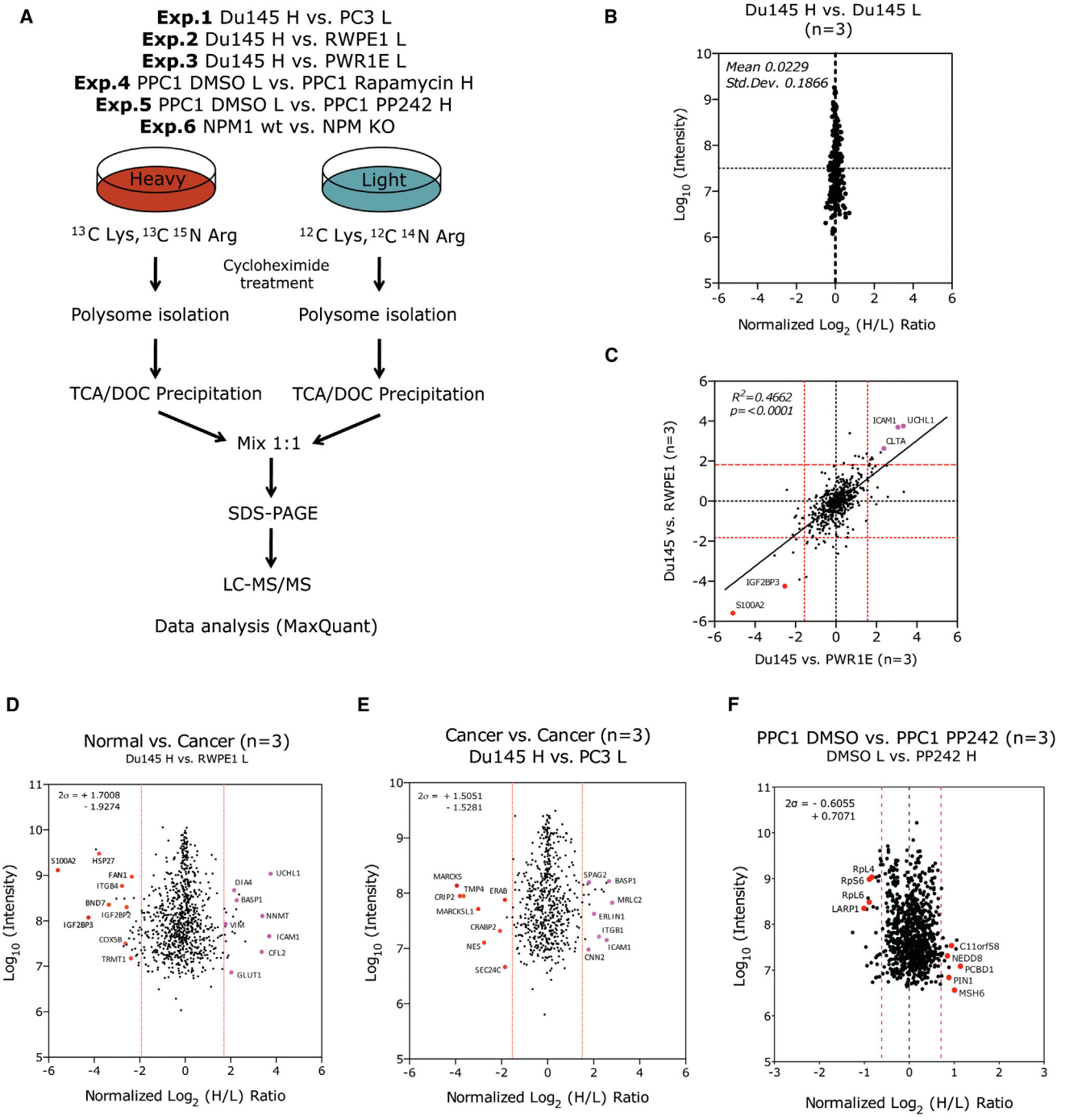

Figure 1. A Quantitative Riboproteomics Approach to Study the Composition of Riboproteomes

(A) Schematic representation of the SILAC-based mass spectrometry experiments.

(B) Scatterplot with normalized Log_2 (H/L) ratios/Log_{10} intensities highlighting the distribution of all quantified proteins between Du145 H- and L-labeled cells. Note that most of the proteins have a ratio of 1:1 between the light and heavy state and therefore have a value close to 0 on a Log_2 axis (mean 0.0229; SD 0.1866).

(C) Standard scatterplot with normalized Log_2 (H/L) ratios comparing the two N/C data sets (RWPE1 versus Du145 and PWR1E versus Du145). All shared proteins between the data sets are plotted. Both data sets show a highly significant positive correlation (R^2 = 0.4662; p = < 0.0001).

(D–F) Standard scatterplots with normalized Log_2 (H/L) ratios/Log_{10} Intensities (Normal versus Cancer n = 3, left panel; Cancer versus Cancer n = 3, middle panel; PPC1 DMSO versus PP242, n = 3, right panel) highlighting the distribution of quantified proteins in each screen (cutoff values for enriched proteins was 2 SDs (2σ) from the mean, dashed red lines). Proteins of interest in either experimental setting are highlighted.

See also Figure S1 and Tables S1, S2, S3, S4, S5, S6, S7, S8, and S9.

(cutoffs are based on two SDs from the mean) (Figures 1D, 1E, and S1D). These differences are described in greater detail below and include a variety of proteins including RBPs (e.g., IGF2BP2, IGF2BP3), cell adhesion molecules (e.g., Integrin β1), and signaling proteins (e.g., MARCKS) among others.

In addition, acute exposure to the mTOR inhibitors rapamycin and PP242 in PPC1 cells reveals that only strong inhibition of the mTOR kinase itself results in a clear perturbation to the riboproteome (Figures 1F and S1E). This is consistent with the differential capacity of these drugs to inhibit mTOR activity toward translation (DMSO < rapamycin < PP242) with numerous ribosomal proteins and RBPs (e.g., RpL4, RpL6, RpS6, LARP proteins), demonstrating the most striking quantitative differences (Figures 1F and S1E).

Comparing *Npm1* wild-type or null immortalized MEFs, we combined mass spectrometry data from two separate biological replicates, including a label switch. No change in relative quantification of ribosomal proteins was observed between *Npm1* wild-type and null immortalized MEFs (Figure S1F). Interestingly, *Npm1* was identified as the most highly decreased protein in *Npm1*-null riboproteomes (Figure S1F), due to the presence of N-terminal peptides that remain as a result of the knockout strategy (Grisendi et al., 2005), thereby serving as an internal positive control.

Notably, our approach identified and quantified all but one (RpL41, a lysine- and arginine-rich 25 amino acid protein that is unlikely to be identified by this mass spectrometry approach due to the large number of sites available for trypsin cleavage, and the consequent inability to generate multiple peptides) ribosomal protein (Figure S1G), as well as other known translation-associated proteins including initiation and elongation factors (see Tables S3, S4, S5, S6, S7, and S8). We observed that ribosomal proteins of both the small and the large subunit cluster around a normalized Log_2 (H/L) = 0 (Figure S1H), indicating that ribosomal proteins are unchanged between normal and cancer cells, as well as between cancer cell lines and genetically defined MEFs. These data make the important point that, at least among these cell lines, core ribosomal protein composition in polysomes is not altered.

Characterization of the Riboproteome

Overall, the number of proteins quantified in each of the individual groups of experiments varied from 575 to 991 (Figure S2A) and offered the potential to uncover a significant overlap of proteins that makes up the riboproteomic space in mammalian cells.

To first examine how the data sets compared to one another, we carried out an unsupervised hierarchical clustering of the six conditions analyzed (Figure S2B). Interestingly, the MEF data set appeared to cluster independently from the human prostate cancer cells, whereas, among the prostate cancer cells, PPC1 cell lines cluster together and the immortalized prostate epithelial cell lines cluster together. The PC3 and Du145 experiments displayed greater similarity to immortalized epithelial cells, likely due to their shared comparison. These data indicate that the riboproteome itself may have the capacity to categorize cell types and tissues based on riboproteomic diversity, and, in turn, can contribute to regulation of gene expression within a given cellular compartment.

In addition to a number of significant differences identified between the various samples, the hierarchical clustering clearly demonstrated all prostate cell lines shared high similarity. Thus, we chose to combine these data sets in order to gain a global perspective of the prostate riboproteome. In the combined prostate cell line data set, we identified a total of 1,499 quantified proteins (Figure 2A; Table S9). Of these 1,499 proteins, 70% were identified in at least two experimental data sets, whereas 24% (363 of 1,499) were identified in all five experiments (Figure 2B; Table S9). Indeed, this number of 363 core riboproteomic components represents over 60% of the PC3/Du145 SILAC experiment, which contained the lowest number of proteins identified in the prostate cell line cohort (Figure S2A). It is also interesting to note that 96% of proteins quantified in this PC3/Du145 data set were found in at least one other data set, with only 21 proteins quantified unique to this experiment (Figure S2; Table S9). These data show strong overlap in proteins identified among the independent riboproteome experiments and highlight the advantage of using multiple cell lines to characterize the riboproteome.

We subsequently carried out Ingenuity Pathway Analysis (http://www.ingenuity.com/) of all 1,499 proteins identified to examine what (1) biological functions and (2) canonical pathways may be specifically enriched in our data set. Importantly, we found biological functions related to protein synthesis, post-translational modification, and protein folding to be highly enriched in our combined data set (Figure S2D). In agreement with this, the canonical pathway analysis demonstrated EIF2 signaling, regulation of eIF4 and p70S6K signaling, and mTOR signaling pathways to be significantly represented (Figure S2E).

In addition, KEGG pathway analysis of proteins identified in all five experimental data sets (363/1,499) compared to proteins identified in at least one experiment (1,499) identified ribosome related pathways to be highly enriched (Figure S2F).

Diversity of Protein Functional Groups and Enrichment of RNA Binding Proteins in the Riboproteome

To better understand the various protein components that make up the riboproteome, we used DAVID (david.abcc.ncifcrf.gov) (Huang et al., 2009) to perform a gene ontology-based functional categorization of the proteins identified in our combined data set (Figure 2C). This analysis demonstrated a clear and significant enrichment in ribosome and translation related processes. In addition, a number of other diverse protein functional groups were found to be included in the riboproteome, including melanosome and glucose catabolic processes. Critically, we identified a significant enrichment of RBPs to be constituents of the riboproteome. As two recent papers published now describe the RNA-binding protein interactome in detail (Baltz et al., 2012; Castello et al., 2012), we compared riboproteome and RBP-interactome data sets to evaluate the proportion of RBPs that form part of the riboproteome. Using the data set from Castello et al. (2012), we find a considerable overlap between the RBP interactome and riboproteome (Figure 2D). Strikingly, core riboproteome components show themselves to be enriched in RBP-interactome proteins (50% of proteins identified can be assigned to the RBP interactome, Figure 2E, left panel), whereas those proteins identified in only one experimental condition have a much lower RBP-interactome component (only 29% of

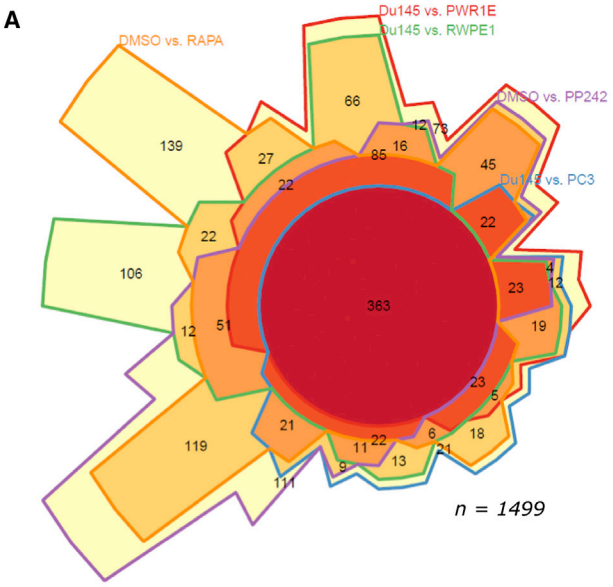

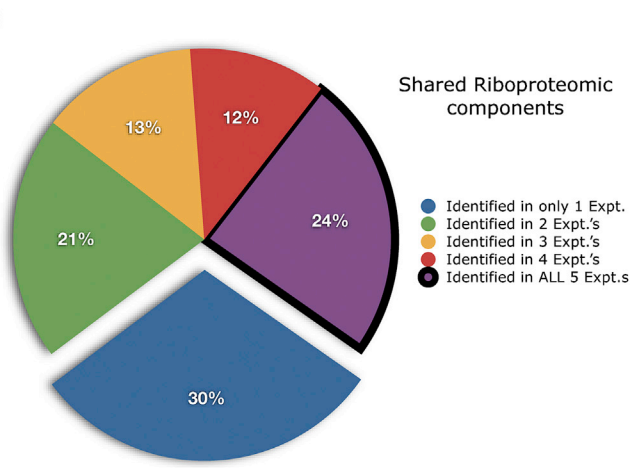

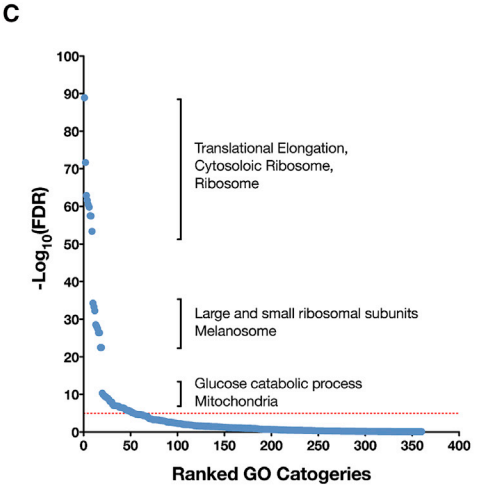

Term	Count	PValue	Fold Enrichment	FDR
translational elongation	70	7.30E-91	29.76	1.24E-87
cytosolic ribosome	57	1.57E-73	29.59	2.12E-70
cytosolic part	65	9.15E-65	17.98	1.24E-61
cytosol	146	1.86E-63	4.62	2.51E-60
translation	83	2.11E-62	10.77	3.57E-59
ribosome	71	1.18E-61	13.88	1.59E-58
structural constituent of ribosome	64	2.06E-59	15.80	3.01E-56
ribosomal subunit	58	2.64E-59	19.05	3.56E-56
ribonucleoprotein complex	92	3.18E-55	7.51	4.30E-52
cytosolic large ribosomal subunit	28	3.89E-36	30.98	5.26E-33
cytosolic small ribosomal subunit	28	3.72E-35	29.43	5.03E-32
RNA binding	83	3.86E-34	4.79	5.64E-31
structural molecule activity	74	1.90E-30	4.84	2.78E-27
large ribosomal subunit	30	6.62E-30	18.83	8.95E-27
small ribosomal subunit	29	2.61E-29	19.35	3.53E-26
intracellular non-membrane-bounded organelle	147	2.95E-28	2.38	3.98E-25
non-membrane-bounded organelle	147	2.95E-28	2.38	3.98E-25
melanosome	29	2.50E-24	13.70	3.38E-21
pigment granule	29	2.50E-24	13.70	3.38E-21
unfolded protein binding	21	3.33E-12	7.57	4.86E-09

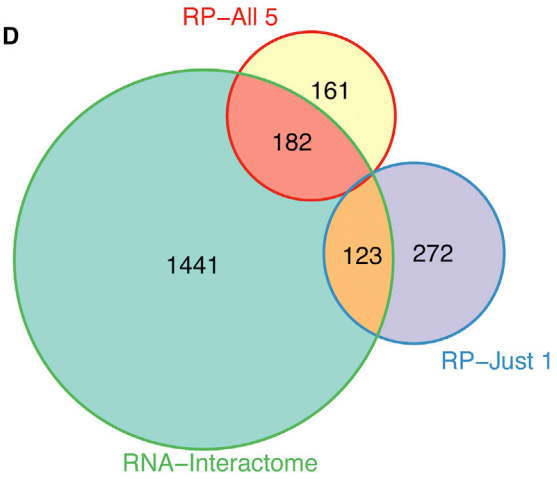

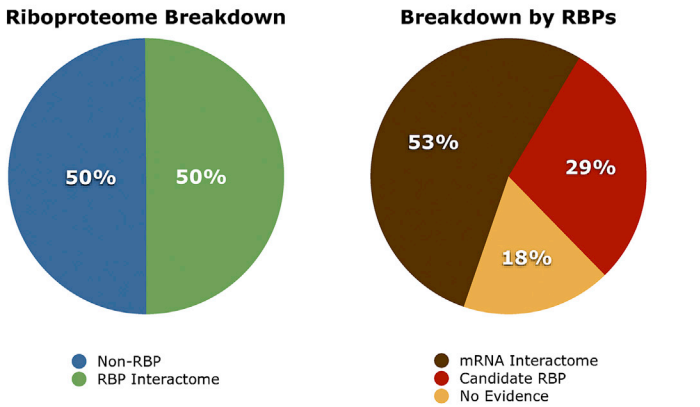

(legend on next page)

proteins identified can be assigned to the RBP interactome, Figure S2H, left panel). Moreover, it is interesting to note that, when we break down our riboproteome RBPs according to the categories defined by Castello et al. (2012) in Figure S2G (i.e., mRNA-interactome; candidate RBP; no evidence), we find that their proportional distribution in these three categories is highly similar to those described by Castello et al. (2012) (Figures 2E and S2H, right panels for RBP categories from the riboproteome).

Riboproteomic Genes Are Frequently Amplified in Human Cancer

As cellular proliferation is strongly coupled to translation, we next evaluated if the riboproteome may be altered in human cancer using the cBio Cancer Genomics Portal (http://cbioportal.org) and the R package *cgdsr*, developed at Memorial Sloan-Kettering Cancer Center.

We first examined the distribution of copy-number alterations in the riboproteome as compared with genes in the background genome across 16 cancer types. This analysis included between 1,661 and 1,720 of the riboproteome genes (median = 1,675) and 19,195 nonriboproteome background genes. The overall analysis shows that the riboproteome is enriched for copy-number gains and high-level amplifications (Figures 3A and S3A) and depleted for hemizygous and homozygous deletions (all $p < 2.2e^{-16}$) (Figures 3B and S3B).

Based on these data, we sought to identify riboproteomic genes that undergo the most frequent copy-number alterations in specific cancer types. This analysis focused on 532 riboproteome genes with complete copy-number data across 15 cancer types. Riboproteome genes were ranked by the maximum number of cases where they showed a genomic amplification across the 15 cancers (Figures 3C and S3C). Interestingly, we observed that 38 riboproteome genes correlated with high-level amplifications in at least 10% of at least one cancer type (Figure 3D). Although several genetic loci are represented in this data set including 4p16.3, 1p33, and 19p13, more than half of these genes (60%, 23 of 38) grouped to three specific genetic loci. These loci represented 1q22, 3q26, and 8q24, with regions surrounding chromosome 3q26 and 8q24 identified as showing most frequent amplification (Figures 3C and 3D). Analysis of the gene signature for the 3q riboproteomic gene locus (nine genes) in the TCGA studies containing mutation data showed that 51% (91 of 178 cases) of lung squamous cell carcinoma contained an alteration in at least one of these genes (Figure 3E, left panel). Ovarian serous cyst adenocarcinoma showed alterations of 39% (Figure 3E, left panel), whereas patient samples from other cancer types also showed alterations in this 3q gene set (Figure 3E, left panel). Analysis of the same data sets for the 8q riboproteome gene locus identified breast invasive carcinoma to harbor frequent alterations to genes in this locus (21% of cases, 103 of 482 cases) (Figure 3F, left panel). Ovarian serous cyst adenocarcinoma patients also showed significant alteration (38%%, 121 of 316 cases), whereas prostate cancer patients showed alteration in 13% of patients at this locus (11 of 82 cases [Figures 3F, left panel and S3E]). Accordingly, closer analysis of 3q26 and 8q24 riboproteome gene groups in individual patients clearly demonstrates frequent coamplification of these genes, in line with our hypothesis that riboproteomic genes are preferentially amplified in cancer (Figures 3E and 3F, right panels). Similarly, the 1q22 locus demonstrates a frequent amplification in various cancer types (Figure S3D).

Interestingly, both 3q26 and 8q24 harbor established oncogenes *PIK3CA* and *MYC*, respectively. Although it may be considered that the riboproteomic genes in these regions may be simply amplified along with the dominant oncogene at the relevant locus, our cBio analysis clearly identifies a number of patients with invasive breast carcinoma without MYC amplification or mutation, while still harboring amplification of 8q24 riboproteome genes (Figure 3F, right panel), suggesting that they have the potential to promote tumorigenesis independent of MYC.

We also noted that the amplified riboproteomic loci were infrequently coamplified in a number of cancer types. For example, limited co-occurrence of 3q26 and 1q22 amplification is observed in patients from lung adenocarcinoma and breast invasive carcinoma cancer data sets (Figures S3F and S3G).

The Riboproteomic Platform for the Identification of Riboproteomic Components and Regulators of Translation

Next, we focused on differences in N/C cells as well as C/C cells to identify riboproteomic components and as a means to validate our approach. As mentioned above, our data sets revealed marked differences in proteins quantified between polysomal fractions of normal and cancer cells (i.e., RWPE1 and PWR1E cells compared to Du145 cells), indicating that the Du145 cancer cells display numerous differences in the composition of their riboproteome (Figures 1D and S1D). These differences encompass a variety of protein types and include a number of potential

Figure 2. Analysis of the Prostate Riboproteome

(A) Venn diagram showing how proteins identified in each of the five SILAC experiments utilizing prostate cell lines are shared between each of the individual data sets. Out of total of 1,499 proteins quantified between all experiments, 363 are shared by all five experiments.

(B) Pie chart illustrating the distribution of proteins identified across the various experiments. Proteins identified in a single experiment (30%) are highlighted by the detached blue pie slice, whereas proteins identified in all five experiments (24%) are indicated by a bold border.

(C) Gene ontology (GO) analysis of the prostate riboproteome highlights multiple different pathways and functional groups that are significantly enriched in the riboproteome. A table of significantly enriched GO terms relating to translation identified by DAVID analysis is shown.

(D) Venn diagram indicating the extent of overlap between the RNA binding protein (RBP) interactome identified by Castello et al. (2012) and the riboproteome constituents described here.

(E) Pie charts to illustrate the extent to which components of the RBP interactome overlap with the riboproteome. The left panel shows the percentage of identified proteins that are also called within the Castello et al. (2012) data set for the core riboproteomic data set (i.e., identified in all five experiments). Right panel illustrates how the RBP-interactome components identified in the riboproteomic data set are distributed among the various RBP-interactome categories defined by Castello et al. (2012).

See also Figure S2.

Cell PRESS
Open ACCESS

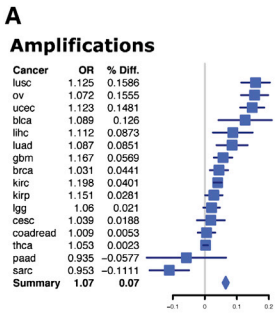

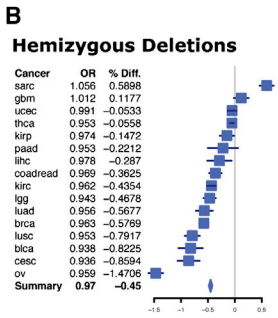

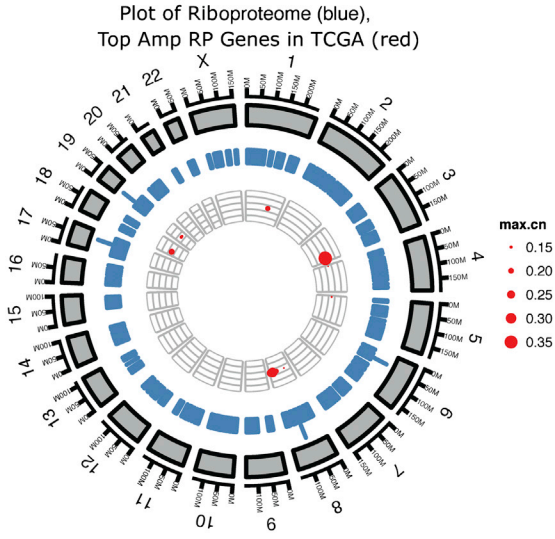

D

Approved Symbol	Approved Name	Chr Location	HGNC
FXR1	fragile X mental retardation, autosomal homolog 1	3q28	4023
GFM1	G elongation factor, mitochondrial 1	3q25	13780
GMPS	guanine monphosphate synthetase	3q25.31	4378
KPNA4	karyopherin alpha 4 (importin alpha 3)	3q25.33	6397
MRPL47	mitochondrial ribosomal protein L47	3q26.33	16652
NCEH1	neutral cholesterol ester hydrolase 1	3q26.31	29260
PSMD2	proteasome (prosome, macropain) 26S subunit, non-ATPase, 2	3q27.3	9559
TFRC	transferrin receptor (p90, CD71)	3q26.2-qter	11763
UBXN7	UBX domain protein 7	3q29	29119
FAM49B	family with sequence similarity 49, member B	8q24	25216
MTDH	metadherin	8q22.1	29608
PABPC1	poly(A) binding protein, cytoplasmic 1	8q22.2-q23	8554
PLEC	plectin	8q24	9069
POP1	processing of precursor 1, ribonuclease P/MRP subunit (S. cerevisiae)	8q22.2	30129
PUF60	poly-U binding splicing factor 60KDa	8q24.3	17042
TSTA3	tissue specific transplantation antigen P35B	8q24.3	12390
YWHAZ	tyrosine 3-monooxygenase/tryptophan 5-monooxygenase activation protein, zeta polypeptide	8q22.3	12855
HIST2H2BF	histone cluster 2, H2bf	1q21.2	24700
PFDN2	prefoldin subunit 2	1q23.3	8867
PSMB4	proteasome (prosome, macropain) subunit, beta type, 4	1q21	9541
PSMD4	proteasome (prosome, macropain) 26S subunit, non-ATPase, 4	1q21.2	9561
TAGLN2	transgelin 2	1q21-q25	11554
UAP1	UDP-N-acteylglucosamine pyrophosphorylase 1	1q23.2	12457
PRKACA	protein kinase, cAMP-dependent, catalytic, alpha	19p13.1	9380
RAB8A	RAB8A, member RAS oncogene family	19p13.2-p13.1	7007
RAD23A	RAD23 homolog A (S. cerevisiae)	19p13.2	9812
TPM4	tropomyosin 4	19p13.1	12013
MYCBP	c-myc binding protein	1p33-p32.2	7554
PABPC4	poly(A) binding protein, cytoplasmic 4 (inducible form)	1p34.2	8557
PPT1	palmitoyl-protein thioesterase 1	1p32	9325
LETM1	leucine zipper-EF-hand containing transmembrane protein 1	4p16.3	6556
TACC3	transforming, acidic coiled-coil containing protein 3	4p16.3	11524
MIB1	mindbomb E3 ubiquitin protein ligase 1	18q11.2	21086
SNRPD1	small nuclear ribonucleoprotein D1 polypeptide 16kDa	18q11.2	11158
PDCD5	programmed cell death 5	19q12-q13.1	8764
PSMD8	proteasome (prosome, macropain) 26S subunit, non-ATPase, 8	19q13.2	9566
PROSC	proline synthetase co-transcribed homolog (bacterial)	8p11.2	9457
NDUFB9	NADH dehydrogenase (ubiquinone) 1 beta subcomplex, 9, 22kDa	8q24.13	7704

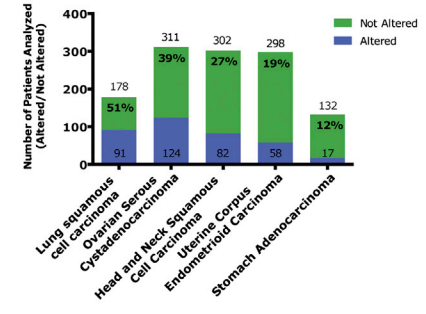

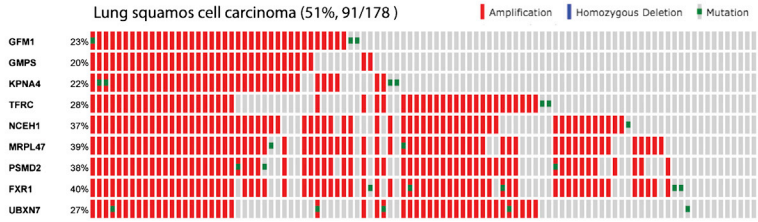

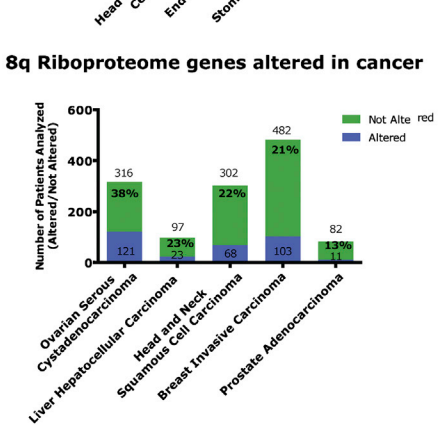

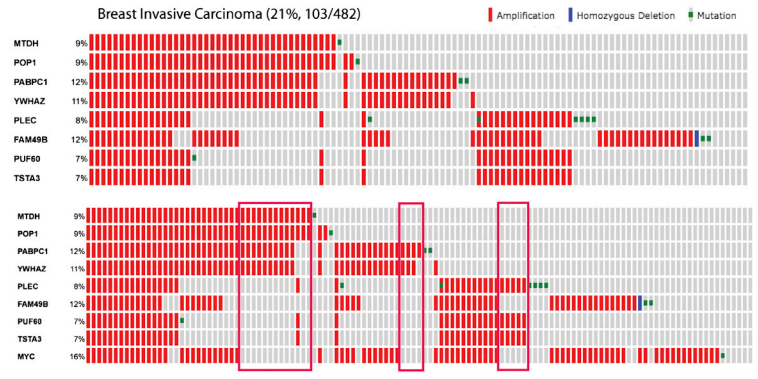

(legend on next page)

ribosome-associated proteins that were reproducibly enriched on the polyribosomes of either normal or cancer cells, including intracellular adhesion molecule 1 (ICAM1), vimentin (VIM), and Integrin β1 (ITGB1) that are enriched in cancer cells as well as the RBPs IGF2BP2 and IGF2BP3 that were among others reproducibly enriched in normal cells (Figures S4A and S4B; Tables S3 and S4). In order to further establish the relevance of the riboproteome in the context of cancer, we focused on differentially quantified proteins associated with polyribosomes of prostate cancer cells (i.e., PC3 cells compared with Du145 cells) (Figures 1E and S4C; Table S5).

Among these differentially quantified proteins, MARCKS stood out as it was a highly differential factor (Figures 1E and S4C) and a major cellular substrate for protein kinase C (PKC), suggesting that MARCKS might represent a regulator of cellular translation and a candidate for further validation.

Importantly, MARCKS was strongly associated with polyribosomes of the prostate cancer cell line PC3 when compared to Du145 cells (Figure 4A). To further confirm this observation, we isolated polysomal fractions from three prostate cancer cell lines (PC3, PPC1, and Du145) as well as the two normal immortalized-epithelial control cell lines (PWR1E, RWPE1) and subjected pooled polysomal fractions to western blot analysis. Indeed, we were able to confirm that PC3 and PPC1 cells displayed increased amounts of MARCKS on polyribosomes when compared to either Du145 or prostatic epithelial cell lines (Figure 4B). In addition, these cells also displayed high levels of phosphorylation of the PKC sensitive serine residues of MARCKS (S159 and S163) (Figure 4B). This analysis also validated our SILAC findings that ribosomal protein levels (e.g., RpS6, RpS14, and RpL7a) remain unaltered between cancer cell lines (Figure 4A). In contrast to MARCKS, our SILAC analysis revealed that Integrin β1 was highly enriched in Du145 cells when compared to PC3 cells, and western blot analysis also confirmed this differential enrichment (Figure 4A).

To extend this validation and analysis further, we carried out additional western blot analysis on lysates from each of the prostate cell lines utilized in this screening. As expected, we were able to confirm the presence of all proteins analyzed in the polysomal fractions collected (Figure 4C). Additionally, these data confirm the SILAC predictions regarding differential expression of proteins (e.g., compare Integrin β1 in PC3 and Du145 lysates, or IGF2BP3 in Du145 and RWPE1 lysates, Figure 4C).

As an additional validation for polysomal association, we employed a well-established method of puromycin-mediated dissociation of ribosome-mRNA complexes (Blobel and Sabatini, 1971). As shown in Figure S4E, puromycin treatment results in the loss of RpS6 and RpL13a from polyribosomes as determined by western blot analysis of pooled polysomal fractions. As an example of a riboproteome component associating with polyribosomes, the presence of MARCKS was also dramatically decreased in polyribosome fractions upon puromycin treatment (Figures 4D and S4E), which in addition supports the hypothesis that MARCKS plays a role in translation through association with actively translating ribosomes.

We next hypothesized that the riboproteomic platform would allow for the identification of mechanisms of response to pharmacological perturbation and for translational targets that could be differentially exploited for therapeutic intervention in cancer.

To this end, we performed riboproteomic analysis upon inhibition of mTOR using the inhibitors rapamycin (a TORC1 inhibitor [Thoreen and Sabatini, 2009]) and PP242 (a mTOR kinase inhibitor that inhibits TORC1 and TORC2 activity simultaneously [Feldman et al., 2009]) as mentioned above. This analysis revealed that the riboproteome is indeed differentially responsive to treatment modalities. Although, we find that rapamycin has little impact on the composition of the riboproteome (Figure S1E; Table S6), the more potent mTOR kinase inhibitor PP242 results in a much stronger and more robust perturbation of the riboproteome (Figure 1F; Table S7). Indeed, although inhibition of mTOR by PP242 identifies a number of proteins, including some ribosomal proteins (e.g., see RpL4, RpL6, and RpS6 in Figure S4D; Table S7) that show a rapid and significant disassociation from the riboproteome upon treatment with PP242, this may represent a more general dissociation of the ribosome and a block in translation. Interestingly, the RBP LARP1 (*La ribonucleoprotein domain family member 1*) appeared to be one of the most dynamic components of the riboproteome in response to mTOR inhibition by PP242 (Figures 1F and 4E). Although the function of LARP1 is not completely understood, it has been reported to play a role in cell division, apoptosis, and migration (Burrows et al., 2010), and it has been shown to be an mTOR-sensitive phosphoprotein (Hsu et al., 2011; Yu et al., 2011). We confirmed the RNA binding activity of LARP1 (Burrows et al., 2010), by using a micrococcal nuclease (MN) assay (Darnell et al., 2011). Pooled sucrose gradient fractions containing LARP1 protein were treated with and without MN. Ribosomes were subsequently pelleted by ultracentrifugation, and the protein in supernatant and pellet were isolated for western blot

Figure 3. Alterations to the Riboproteome in Cancer

(A) Forest plot highlighting the enrichment of amplifications among riboproteomic genes when compared to background genes in the cBio TCGA data set.

(B) A similar forest plot demonstrating significantly less heterozygous deletions among riboproteomic genes in the cBio TCGA data set when compared to background genes.

(C) Circos plot to illustrate the distribution of all riboproteomic components across the genome. Blue bars represent individual riboproteomic components, and their genomic localization, whereas internal red regions highlight genomic regions containing riboproteome genes found to be most frequently amplified in the TCGA repository.

(D) Table detailing the top amplified genes as identified in the TCGA repository and organized according to genomic loci.

(E and F) Summary from the TCGA for riboproteome genes in the regions of 3q and 8q, respectively, that are found to be frequently amplified in human cancer. Left panels show the number of patients harboring an alteration from the data sets analyzed. As lung squamous cell carcinoma for the 3q locus and breast invasive carcinoma for the 8q locus were found to show high levels of alteration in both cases, the right panels illustrate the types of alteration found in these patients (amplification, homozygous deletion, or mutation).

See also Figure S3.

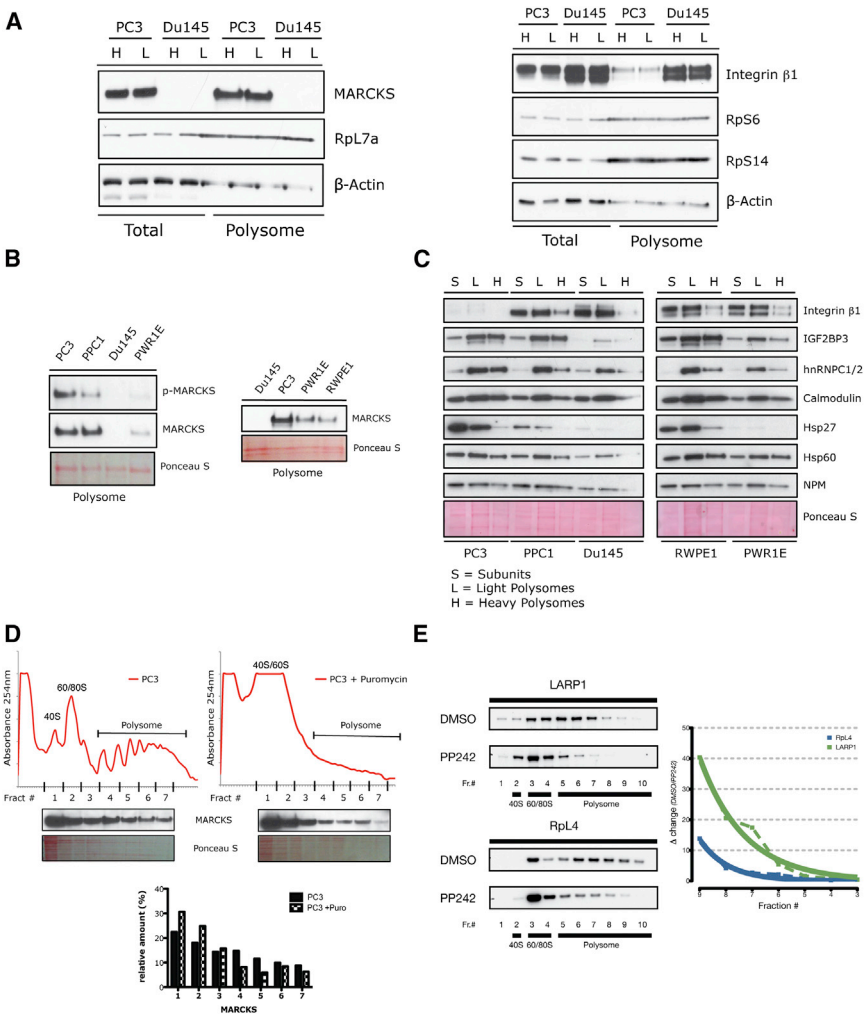

Figure 4. Riboproteomics Uncovers Ribosome-Associated Proteins

(A) Western blot analysis of total lysates and polysomal fractions from PC3 and Du145 H- and L-labeled cell lines. Western blots for MARCKS, RpL7a, Integrin β1, RpS6, RpS14, and β-actin are shown.

(B) Western blot analysis of pooled polysomal fractions showing differential enrichment of phospho-MARCKS and MARCKS from ribosomes of Du145, PC3, PWR1E, and RWPE1 cells (right panel) and PC3, PPC1, Du145, and PWR1E cells (left panel). Ponceau S staining served as a loading control.

(C) Western blot analysis from pooled polysomal fractions validating ribosome-associated proteins from ribosomes of PC3, PPC1, Du145, RWPE1 and PWR1E cells. For this analysis, polyribosomes have been isolated from all cell lines and fractions have been pooled to obtain subunits (S, fractions #3-5, see Figure S1A), early light polysomes (L, fractions #6-8, see Figure S1A) and late heavy polysomes (H, fractions #9-11, see Figure S1A). Western blots for Integrin β1, IGF2BP3, hnRNPC1/2, Calmodulin, Hsp27, Hsp60 and NPM are shown. Ponceau S staining served as a loading control.

(D) PC3 prostate cancer cells were subjected to puromycin-mediated dissociation of ribosome-mRNA complexes to demonstrate a specific association of MARCKS with the ribosome. Protein was isolated from individual fractions (#1–#7) of the sucrose gradients using TCA/DOC precipitation and subjected to western blot analysis for MARCKS. The relative distribution of MARCKS across the sucrose gradient was quantified using the ImageJ software (http://rsbweb.nih.gov/ij).

(E) Western blot analysis from protein isolated from individual fractions across the sucrose gradients of PPC1 cell lysates treated with DMSO or PP242. Shift in LARP1 (upper left panels) and RpL4 (lower left panels) proteins can be readily observed upon treatment with the mTOR kinase inhibitor. Right panel: rate of change between DMSO and PP242 conditions for LARP1 (green) and RpL4 (blue) from late to early fractions (#9–#3).

See also Figure S4.

analysis. As seen in Figure S4F, LARP1 behaved similar to the well-characterized poly-A binding protein (PABP). Without MN treatment, LARP1 pelleted with ribosomal proteins, indicating its close association with polysome components. However, upon treatment with MN, LARP1 no longer associated with riboproteome components and is released into the supernatant similar to PABP (Figure S4F). This indicates that LARP1 is predominantly an RBP, showing limited association with the ribosome itself. In addition, treating cells with PP242 prior to this analysis, we observed that, whereas PABP appears to remain tightly intact with polysome fractions, there appears to be more LARP1 observed in the supernatant, suggesting that mTOR inhibition can selectively influence binding of LARP1 at the polysome (Figure S4G). Thus, these findings suggest that mTOR activity toward LARP1 may represent an additional means by which mTOR can regulate translation.

Finally, to examine whether the riboproteome is altered in response to a genetic perturbation, we carried out SILAC riboproteomic analysis on *Npm1* wild-type and null immortalized MEF (immortalized by deletion of the *Trp53* gene) (Figure S1F). Again, SILAC analysis of polysome fractions demonstrated a high similarity between riboproteome components, with ribosomal proteins themselves showing no quantitative difference between the *Npm1* wild-type or null MEF preparations (Figure S1F; Table S8). However, there were a number of proteins that demonstrated differential association with polysomes from *Npm1* wild-type and null MEFs, which may be relevant for translation in these cells (Figures S1F and S4H). Interestingly, we identified the heterogeneous nuclear ribonucleoprotein hnRNPC to be one of the most highly increased proteins on the polysomes of *Npm1*-null MEFs (Figure S4I; Table S8).

Thus, taken together these data validate this approach as an effective means to study riboproteome composition in a wide variety of cellular contexts and highlight this approach as a valuable resource that can be applied to the study of how perturbations to genes and pathways impact the riboproteome.

DISCUSSION

Over the last number of years, there has been increasing awareness of the role that ribosome, ribosome biogenesis, and various other factors that relate to translation play in normal cellular homeostasis, and in human disease (Xue and Barna, 2012). However, there is a pressing need to understand in greater detail the many factors that contribute to ribosome function and the regulation of translation on a global scale. Thus, we set out to analyze in a nonbiased, high-throughput manner the numerous factors that coordinate ribosome function and mRNA translation. Here, we present an overview of the riboproteome, as characterized by analysis of several different cell lines and different cellular contexts.

The general overview described here allowed us to draw a number of important conclusions relating to the various elements that make up the riboproteome and allowed us to gain new insight into how the ribosome and translation is regulated.

First, by cross-referencing data from independent SILAC riboproteomic experiments, and using a comprehensive panel of prostate cell lines, we were able to identify a core group of proteins that are consistently identified in all experimental data sets, whereby at least 70% of proteins quantified were found in at least two experimental data sets. From this global analysis, we show that our data set is highly enriched in factors that relate directly to the ribosome, to translational initiation and elongation, and to pathways that are known to regulate and control translation. Importantly, this comprehensive analysis also reveals that the riboproteome consists of significant proportion of RBPs. As recently reported, the mRNA-interactome revealed that a wide variety of proteins previously unappreciated as RBPs can bind to mRNA (Castello et al., 2012; Baltz et al., 2012). This diversity of RBP functionality is also observed in those RBPs represented in our data set. However, there is also a large proportion of proteins that we identify, even as core riboproteome components, that are not annotated as having RNA binding properties, indicating a further layer of functional complexity in those proteins that work to regulate ribosome function and translation.

Second, our data sets indicate that the diversity within the riboproteome itself may have the capacity to categorize cell types and tissues and, importantly, may specifically contribute to regulation of gene expression within a given cellular compartment. Surprisingly, in the data sets we have analyzed the plasticity of the riboproteome does not appear to extend to individual ribosomal proteins themselves that are evenly represented in the various cell types investigated, and they appear to be uniformly altered in response to conditions that impact ribosomal translation, such as mTOR inhibition.

Third, by examining globally how the riboproteome may be altered in diseases such as human cancer, we have made further unexpected observations. We find that riboproteomic components display frequent copy-number amplifications in human cancer, whereas genomic losses within the riboproteome are significantly less than that for nonriboproteomic genes. We further identified three genomic loci around 3q26, 8q24, and 1q22 containing genes that appear to be altered in a significant number of patients for several of the cancer subtypes contained in the cBio TCGA database. It is worth noting that both the regions 3q26 and 8q24 contain the oncogenes *PIK3CA* and *MYC*, respectively. Although *MYC* and *PIK3CA* are frequently amplified in cancer (Beroukhim et al., 2010; Brown et al., 2012; Kolasa et al., 2009), there are several examples within the cBio data sets that the riboproteomic genes within these regions may be amplified without coamplification of the resident oncogene. It is also interesting to note that both MYC and the PI3-kinase signaling pathway represent important regulators of translation themselves.

Fourth, in addition to characterizing the riboproteome landscape in various cell types, we identified and validated a number of proteins previously not known to be associated with actively translating ribosomes (e.g., MARCKS, Integrin β1, and IGF2BP3). These proteins represent a number of interesting ribosome interactors and highlight the diversity of proteins that actually participate in translation. In addition, they also point to the potential of these data sets to identify novel regulators of translation. Definitive riboproteome categorization of each protein identified will require validation as has been carried out for proteins in this study, to fully endorse them as bona fide components of the riboproteome. Although given the high enrichment for RBPs, elongation/initiation factors, and known ribosome biogenesis proteins, it is likely that many of these unexpected proteins are true riboproteome components.

Last, our data demonstrate that the cancer riboproteome can be pharmacologically modulated for therapy on the basis of this molecular knowledge. On the one hand, we show that the riboproteome responds dynamically and differentially to cancer drugs (e.g., rapamycin versus PP242), whereas, on the other hand its differential composition could be used to tailor therapies and predict outcomes based on the riboproteomic profile of specific cell types.

Thus, quantitative, high-throughput riboproteomics represents a powerful platform that can be readily applied to various cellular models to uncover how riboproteome composition contributes to organismal function and disease.

EXPERIMENTAL PROCEDURES

SILAC Labeling and Mass Spectrometry

Metabolic labeling of prostate cell lines (PC3, PPC1, Du145, RWPE1, and PWR1E) and MEFs was carried out using either normal arginine and lysine or heavier isotopic variants of the two amino acids (L-lysine 2HCL [U-13C6], L-arginine HCL [U-13C6, U-N15N4]) (Ong et al., 2002) using Invitrogen's SILAC-FLEX Media kits. SILAC-labeled protein mixtures were run by SDS-PAGE, and gel lanes were cut into eight sections for overnight digestion at pH 8.0 with modified sequencing grade trypsin (Promega). Peptide mixtures were eluted, and each gel section was analyzed separately by microcapillary LC-MS/MS using the EASY-nLC nanoflow HPLC (Thermo Fisher Scientific) with a 75 μm inner diameter × 15 cm length Picofrit capillary column (New Objective) self-packed with 5 μm Magic C_{18} resin (Michrom Bioresources) coupled to a hybrid LTQ Orbitrap XL-ETD mass spectrometer (Thermo Fisher Scientific). The LTQ Orbitrap XL was operated in data-dependent acquisition Top 5 mode (1 profile FT-MS spectrum followed by six centroided IT-MS/MS spectra). The resolution was 30,000 in FT-MS mode and MS/MS spectra were read out at low resolution in the LTQ XL ion trap. The gradient consisted of 3%–38% acetonitrile in 0.1% formic acid (FA) at a flow rate of 300 nl/min for 75 min, 38%–95% acetonitrile in 0.1% FA for 2 min and held at 95% acetonitrile in 0.1% FA at for 7 min followed by column reequilibration for 10 min at 3% acetonitrile in 0.1% FA. MS/MS fragmentation spectra were searched for protein identification using the Andromeda search engine

(http://www.andromeda-search.org) (Cox et al., 2011) against the reversed and concatenated IPI_HUMAN protein database (v3.87) (http://www.ebi.ac.uk/IPI/IPIhuman.html). Carbamidomethylation of cysteine was set as fixed modification and variable modifications were oxidation of methionine and protein N-acetylation. Raw files for SILAC ratio analysis from each experiment were combined and processed using MaxQuant v1.2.2.5 software (http://www.maxquant.org/) (Cox and Mann, 2008). Initial peptide mass tolerance was set to 12 ppm, and fragment ion mass tolerance was set to 0.8 Da. Two missed cleavages were allowed and the minimal length required for a peptide was six amino acids. One unique peptide was required for high-confidence protein identifications and a minimum ratio count of two peptides (one unique and one razor) were required for SILAC ratio determination. The peptide and protein false discovery rates (FDR) were set to 0.01. Normalized SILAC ratios (H/L) were used for subsequent analysis.

Polysome Isolation and Analysis

Polysome profiles were prepared from MEFs and different prostate cancer cell lines as follows. MEFs were seeded at 2×10^6 cells/15 cm and PPC1, PC3, Du145, RWPE1, and PWR1E cells seeded at 10×10^6 cells/15 cm dish and cultured overnight to ensure subconfluent cultures for polysome analysis. PPC1 cells were treated the following day with either DMSO, rapamycin (20 nM) or PP242 (500 nM) for 3 hr. For polysome preparation, cells were then incubated with cycloheximide at a final concentration of 100 μg/ml for a period of 15 min. Plates were then washed with ice-cold PBS containing 100 μg/ml cycloheximide (PBS/CHX), scraped, and collected in ice-cold PBS/CHX. Cells were pelleted by centrifugation and subsequently lysed in polysome lysis buffer (20 mM Tris-HCl [pH 7.4]; 5 mM $MgCl_2$; 150 mM NaCl; 1% Triton X-100; 1% deoxycholate; 2.5 mM DTT; 200 U/ml RNasin; 100 μg/ml cycloheximide; 1 × complete, EDTA-free protease inhibitor cocktail [Roche]; 1 × protease inhibitor set [without EDTA] [G-Biosciences]; α_1-antitrypsin [EMD Biosciences]) and incubated on ice for 10 min with occasional mixing. Extensive optimization of cell lysis was carried out to identify suitable lysis buffer conditions that completely blocked protein degradation from endogenous proteases, and we found it necessary to include the extensive array of protease inhibitors provided in the G-Biosciences protease inhibitor set. Lysates were centrifuged at 7,000 rpm for 5 min at 4°C, and the supernatant carefully removed. Protein concentrations for lysates were measured by Bradford assay, and equal amounts of protein loaded on a 15%–50% sucrose gradient containing 100 μg/ml cycloheximide, 0.2 mg/ml heparin, and 1 mM DTT. Gradients were centrifuged at 36,000 rpm for 3 hr at 4°C in a Beckman SW40 rotor and subsequently fractionated using an ISCO-Foxy Jr. fraction collector. Polysome profiles were reordered using a UA-6 absorbance detector connected to the fraction collector and measuring absorbance at 254 nm.

Puromycin-induced polysome dissociation was carried out by the addition of 1 mM puromycin directly to the lysis buffer lacking cycloheximide as previously described (Blobel and Sabatini, 1971; Fuchs et al., 2011). Briefly, following lysis, the samples were incubated at 37°C for 15 min to dissociate ribosome-mRNA complexes. Lysates were centrifuged at 13,000 rpm for 5 min at 4°C, and the supernatant was carefully removed and loaded on a 15%–50% sucrose gradient. Gradients were centrifuged and fractionated as described above.

Bioinformatics Analysis of the Riboproteome

To cluster riboproteome experiments based on the riboproteins identified in each experiment, we created a Boolean matrix of riboproteome genes by riboproteome experiments, in which each entry in the matrix was a 1 if the row's gene was identified in the column's experiment, and a 0 otherwise. Clustering of the experiments was then performed using a binary distance measure to compute the distance matrix and average linkage for hierarchical clustering, implemented with the R functions *dist* and *hclust*.

Venn diagrams indicating membership of riboproteome genes to SILAC experiments were created using the *Vennerable* package in R.

To identify functional gene sets enriched in the riboproteome genes, we uploaded the riboproteome genes to Ingenuity Pathway Analysis (http://www.ingenuity.com) and identified the top biological functions gene sets and canonical pathways gene sets enriched in the riboproteome gene set. To identify KEGG pathways specifically enriched in the subset of riboproteome genes identified in five of five experiments as compared with the set identified in only one of five experiments, we uploaded the five of five experiments gene list to DAVID and used the one of five experiments gene list as background.

Gene ontology analysis was carried out using the online DAVID bioinformatics resource tool.

TCGA-Based Analyses of Riboproteome Genomic Alterations across Human Cancers

To analyze global patterns of copy-number alterations in the riboproteome versus the background protein-coding genome, we used the *cgdsr* package in R to download Gistic copy-number alteration calls from the 16 cancer types with available data for a large portion of the riboproteome (between 1,661 and 1,720 of the riboproteome genes analyzed for each cancer type, median = 1,675) and the background protein coding genome (19,195 genes). For each cancer type, we recorded the number of homozygous deletions (GISTIC score = −2), hemizygous deletions (GISTIC score = −1), diploid (GISTIC score = 0), low-level copy-number gain (GISTIC score = 1), and high-level amplification (GISTIC score = 2) among the riboproteome genes and among the background genome. We compared the proportion of each of the GISTIC scores observed among the riboproteome genes to the proportion observed among the background protein-coding genome using the function *prop.test* in R. To visualize and summarize the distribution of the proportions of alterations across the cancer types, we created forest plots using the *rmeta* package.

After characterizing the global properties of riboproteome genomic alterations in human cancers, we performed gene-level analyses. At the time of analysis, the cBio Cancer Genomics Portal contained five published data sets and 15 provisional data sets from The Cancer Genome Atlas (TCGA) profiling efforts (Cerami et al., 2012). Although the five published data sets contain mutation data, the provisional TCGA data sets do not.

These analyses were limited to the 532 riboproteome genes with valid data across 15 TCGA cancer types. For each gene, we computed the proportion of cases of each cancer type that the gene showed homozygous deletion, hemizygous deletion, diploid, low-level amplification, and high-level amplification, based on GISTIC calls downloaded via *cgdsr*. For each riboproteome gene, we computed its maximum proportion of each type of alteration across the TCGA cancer types. Riboproteome genes and locations of riboproteome genes undergoing frequent amplifications in cancer were visualized with Circos-like plots, implemented using *ggplot* in R.

Western Blot Analysis

Cells were lysed in lysis buffer containing Complete Mini protease inhibitors (EDTA free) (Roche) and a Phosphatase Inhibitor cocktail (Thermo Scientific). Total protein (5–50 μg) was subjected to SDS-PAGE on 4%–12% Bis-Tris acrylamide NuPAGE gels in MOPS SDS running buffer (Invitrogen). The following primary antibodies were used: MARCKS, phospho-MARCKS (S152/156), Integrin β1, Calmodulin, Hsp27, Hsp60, RpL13a, RpL7a, and RpS6 (all Cell Signaling Technology), HSP90 (BD Biosciences; BD Transduction Laboratories), hnRNPC1/C2 (Millipore), and Rps14 and β-actin (all from Santa Cruz Biotechnologies). The NPM1 antibody was from DAKO and the IGF2BP3 antibody was from ProteinTech. Subsequently, membranes were incubated with secondary HRP-tagged antibodies (Amersham), and signals were visualized with ECL or ECL plus (Amersham). It is important to note that we used Ponceau S staining as a control for equal protein loading in our western analysis of polysomal fractions, because typical housekeeping genes like β-actin or α-tubulin are not enriched in riboproteome preparations and therefore only barely detectable in polysome fractions (Figure 4A; data not shown).

For further details on the materials and methods used in this study, please see the Extended Experimental Procedures.

SUPPLEMENTAL INFORMATION

Supplemental Information includes Extended Experimental Procedures, four figures, and nine tables and can be found with this article online at http://dx.doi.org/10.1016/j.celrep.2013.08.014.

ACKNOWLEDGMENTS

We would like to thank all Pandolfi laboratory members for critical discussions. We would like to thank Min Yuan of the BIDMC Mass Spectrometry Core for help with sample preparation. This research was supported by NIH grant RC1 DK087679 to P.P.P. M.R. received support from the German Academy of Sciences Leopoldina (Leopoldina Research Fellowship grant number: LPDS 2009-27). U.A. received support from AIRC under grant IG-9408. J.M.A. received support from grants NIH 5P01CA120964-04 and NIH DF/HCC Cancer Center Support Grant 5P30CA006516-46.

Received: October 2, 2012
Revised: July 9, 2013
Accepted: August 7, 2013
Published: September 19, 2013

WEB RESOURCES

The URLs for data presented herein are as follows:

Andromeda search engine, http://www.andromeda-search.org
cBio Cancer Genomics Portal, http://cbioportal.org
ImageJ software, http://rsbweb.nih.gov/ij
Ingenuity Pathway Analysis, http://www.ingenuity.com
IPI_HUMAN protein database (v3.87), http://www.ebi.ac.uk/IPI/IPIhuman.html
MaxQuant v1.2.2.5 software, http://www.maxquant.org

REFERENCES

Baltz, A.G., Munschauer, M., Schwanhäusser, B., Vasile, A., Murakawa, Y., Schueler, M., Youngs, N., Penfold-Brown, D., Drew, K., Milek, M., et al. (2012). The mRNA-bound proteome and its global occupancy profile on protein-coding transcripts. Mol. Cell *46*, 674–690.

Beroukhim, R., Mermel, C.H., Porter, D., Wei, G., Raychaudhuri, S., Donovan, J., Barretina, J., Boehm, J.S., Dobson, J., Urashima, M., et al. (2010). The landscape of somatic copy-number alteration across human cancers. Nature *463*, 899–905.

Blobel, G., and Sabatini, D. (1971). Dissociation of mammalian polyribosomes into subunits by puromycin. Proc. Natl. Acad. Sci. USA *68*, 390–394.

Brown, J.R., Hanna, M., Tesar, B., Werner, L., Pochet, N., Asara, J.M., Wang, Y.E., Dal Cin, P., Fernandes, S.M., Thompson, C., et al. (2012). Integrative genomic analysis implicates gain of PIK3CA at 3q26 and MYC at 8q24 in chronic lymphocytic leukemia. Clin. Cancer Res. *18*, 3791–3802.

Burrows, C., Abd Latip, N., Lam, S.-J., Carpenter, L., Sawicka, K., Tzolovsky, G., Gabra, H., Bushell, M., Glover, D.M., Willis, A.E., and Blagden, S.P. (2010). The RNA binding protein Larp1 regulates cell division, apoptosis and cell migration. Nucleic Acids Res. *38*, 5542–5553.

Castello, A., Fischer, B., Eichelbaum, K., Horos, R., Beckmann, B.M., Strein, C., Davey, N.E., Humphreys, D.T., Preiss, T., Steinmetz, L.M., et al. (2012). Insights into RNA biology from an atlas of mammalian mRNA-binding proteins. Cell *149*, 1393–1406.

Cerami, E., Gao, J., Dogrusoz, U., Gross, B.E., Sumer, S.O., Aksoy, B.A., Jacobsen, A., Byrne, C.J., Heuer, M.L., Larsson, E., et al. (2012). The cBio cancer genomics portal: an open platform for exploring multidimensional cancer genomics data. Cancer Discov. *2*, 401–404.

Cox, J., and Mann, M. (2008). MaxQuant enables high peptide identification rates, individualized p.p.b.-range mass accuracies and proteome-wide protein quantification. Nat. Biotechnol. *26*, 1367–1372.

Cox, J., Neuhauser, N., Michalski, A., Scheltema, R.A., Olsen, J.V., and Mann, M. (2011). Andromeda: a peptide search engine integrated into the MaxQuant environment. J. Proteome Res. *10*, 1794–1805.

Darnell, J.C., Van Driesche, S.J., Zhang, C., Hung, K.Y.S., Mele, A., Fraser, C.E., Stone, E.F., Chen, C., Fak, J.J., Chi, S.W., et al. (2011). FMRP stalls ribosomal translocation on mRNAs linked to synaptic function and autism. Cell *146*, 247–261.

Fabian, M.R., and Sonenberg, N. (2012). The mechanics of miRNA-mediated gene silencing: a look under the hood of miRISC. Nat. Struct. Mol. Biol. *19*, 586–593.

Feldman, M.E., Apsel, B., Uotila, A., Loewith, R., Knight, Z.A., Ruggero, D., and Shokat, K.M. (2009). Active-site inhibitors of mTOR target rapamycin-resistant outputs of mTORC1 and mTORC2. PLoS Biol. *7*, e38.

Fuchs, G., Diges, C., Kohlstaedt, L.A., Wehner, K.A., and Sarnow, P. (2011). Proteomic analysis of ribosomes: translational control of mRNA populations by glycogen synthase GYS1. J. Mol. Biol. *410*, 118–130.

Grisendi, S., Bernardi, R., Rossi, M., Cheng, K., Khandker, L., Manova, K., and Pandolfi, P.P. (2005). Role of nucleophosmin in embryonic development and tumorigenesis. Nature *437*, 147–153.

Grisendi, S., Mecucci, C., Falini, B., and Pandolfi, P.P. (2006). Nucleophosmin and cancer. Nat. Rev. Cancer *6*, 493–505.

Hsu, P.P., Kang, S.A., Rameseder, J., Zhang, Y., Ottina, K.A., Lim, D., Peterson, T.R., Choi, Y., Gray, N.S., Yaffe, M.B., et al. (2011). The mTOR-regulated phosphoproteome reveals a mechanism of mTORC1-mediated inhibition of growth factor signaling. Science *332*, 1317–1322.

Huang, W., Sherman, B.T., and Lempicki, R.A. (2009). Systematic and integrative analysis of large gene lists using DAVID bioinformatics resources. Nat. Protoc. *4*, 44–57.

Jackson, R.J., Hellen, C.U.T., and Pestova, T.V. (2010). The mechanism of eukaryotic translation initiation and principles of its regulation. Nat. Rev. Mol. Cell Biol. *11*, 113–127.

Kharas, M.G., Lengner, C.J., Al-Shahrour, F., Bullinger, L., Ball, B., Zaidi, S., Morgan, K., Tam, W., Paktinat, M., Okabe, R., et al. (2010). Musashi-2 regulates normal hematopoiesis and promotes aggressive myeloid leukemia. Nat. Med. *16*, 903–908.

Kolasa, I.K., Rembiszewska, A., Felisiak, A., Ziolkowska-Seta, I., Murawska, M., Moes, J., Timorek, A., Dansonka-Mieszkowska, A., and Kupryjanczyk, J. (2009). PIK3CA amplification associates with resistance to chemotherapy in ovarian cancer patients. Cancer Biol. Ther. *8*, 21–26.

Narla, A., and Ebert, B.L. (2010). Ribosomopathies: human disorders of ribosome dysfunction. Blood *115*, 3196–3205.

Ong, S.-E., Blagoev, B., Kratchmarova, I., Kristensen, D.B., Steen, H., Pandey, A., and Mann, M. (2002). Stable isotope labeling by amino acids in cell culture, SILAC, as a simple and accurate approach to expression proteomics. Mol. Cell. Proteomics *1*, 376–386.

Spellman, D.S., Deinhardt, K., Darie, C.C., Chao, M.V., and Neubert, T.A. (2008). Stable isotopic labeling by amino acids in cultured primary neurons: application to brain-derived neurotrophic factor-dependent phosphotyrosine-associated signaling. Mol. Cell. Proteomics *7*, 1067–1076.

Thoreen, C.C., and Sabatini, D.M. (2009). Rapamycin inhibits mTORC1, but not completely. Autophagy *5*, 725–726.

Xue, S., and Barna, M. (2012). Specialized ribosomes: a new frontier in gene regulation and organismal biology. Nat. Rev. Mol. Cell Biol. *13*, 355–369.

Yu, Y., Yoon, S.-O., Poulogiannis, G., Yang, Q., Ma, X.M., Villén, J., Kubica, N., Hoffman, G.R., Cantley, L.C., Gygi, S.P., and Blenis, J. (2011). Phosphoproteomic analysis identifies Grb10 as an mTORC1 substrate that negatively regulates insulin signaling. Science *332*, 1322–1326.